PCCP

PAPER

View Article Online
View Journal | View Issue

Cite this: *Phys. Chem. Chem. Phys.*, 2018, **20**, 22187

Experimental strategies for $^{13}C–^{15}N$ dipolar NMR spectroscopy in liquid crystals at the natural isotopic abundance†

Lukas Jackalin,[a] Boris B. Kharkov,[b] Andrei V. Komolkin[c] and Sergey V. Dvinskikh*[ab]

Received 1st July 2018,
Accepted 7th August 2018

DOI: 10.1039/c8cp04161j

rsc.li/pccp

Direct dipolar spin couplings are informative and sensitive probes for a wide range of dynamic processes and structural properties at atomic, molecular and supramolecular levels in liquid crystals and other anisotropic materials. Usually, heteronuclear $^{13}C–^{1}H$ dipolar couplings in liquid crystals with natural ^{13}C abundance are measured. Recording $^{13}C–^{15}N$ NMR dipolar spectra in unlabeled materials is challenging because of the unfavorable combination of two rare isotopes. Here we design and compare various experimental strategies to measure short- and long-range heteronuclear $^{13}C–^{15}N$ dipolar couplings in liquid crystalline samples with high molecular orientational order. New techniques were developed to record ^{13}C and ^{15}N spectra of naturally occurring $^{13}C–^{15}N$ spin pairs with increased signal intensity and spectral resolution while suppressing the signals of the uncoupled isotopes. Highly resolved $^{13}C–^{15}N$ dipolar spectra were recorded within an experimental time of a few hours. Coupling constants in a broad range of 10–1000 Hz between spins separated by up to five chemical bonds and distances of up to 5 Å were measured. Because of their relatively low demands on radio-frequency power levels, the experiments were easy to implement using conventional high-resolution solution-state NMR hardware. Experimental data were compared to the results of density functional theory and molecular dynamics computational analyses. The presented experimental methods to characterize the dipolar couplings in unlabeled materials provide novel routes to investigate molecular structure and dynamics in mesophases.

1. Introduction

Nuclear magnetic resonance (NMR) spectroscopy has been established as a powerful experimental tool in fundamental studies of complex molecular dynamic processes and diverse molecular organization in liquid crystals (LCs).[1] The unique feature of a material in the LC state is that a high degree of molecular mobility, which results in fluidity or plasticity, is combined with partial orientational and positional order. The presence of order in the fluid material leads to unique dynamic properties that have been exploited in diverse technological applications.[2] In NMR spectroscopic studies of LCs and solids, structural and dynamic information is obtained through the measurement of anisotropic spin interactions. In particular, dipolar couplings, which by their nature have well-defined orientational and distance dependence, have proven to be informative and sensitive probes of the molecular conformation, dynamics, local order, and other specific properties of LCs at the atomic, molecular, and supramolecular levels. The progress in methods for spin decoupling/recoupling, sensitivity enhancement, and polarization transfer has considerably increased the potential of dipolar NMR spectroscopy to characterize mesophases.[3] While ^{1}H NMR spectra of LCs lack chemical resolution and exhibit complex ill-resolved spectral shapes, spectra of rare isotopes, such as ^{13}C and ^{15}N, display high resolution and thus provide site-specific information on anisotropic spin couplings. Commonly, heteronuclear $^{13}C–^{1}H$ dipolar couplings in LCs with natural ^{13}C abundance are measured using various two-dimensional (2D) separated local field (SLF) spectroscopy techniques.[3–5] Carbon–deuterium heteronuclear dipolar couplings have also been measured in LC samples with ^{2}H isotopic enrichment;[6–11] however, this approach required synthetically demanding and expensive site-specific isotopic labeling.[12] Dipolar/*J*-coupled $^{2}H–^{13}C$ spectra at natural abundance in weakly ordered liquids have been recorded, taking advantage of the narrow resonances and small splittings.[13]

[a] *Department of Chemistry, KTH Royal Institute of Technology, SE-10044 Stockholm, Sweden. E-mail: sergeid@kth.se*
[b] *Laboratory of Biomolecular NMR, Saint Petersburg State University, Saint Petersburg, 199034, Russia*
[c] *Faculty of Physics, Saint Petersburg State University, Saint Petersburg 199034, Russia*

† Electronic supplementary information (ESI) available. See DOI: 10.1039/c8cp04161j

Nitrogen atoms are typically present in terminal and bridging functional groups of molecules that form thermotropic mesophases.[14] Recording NMR spectra of and measuring coupling to the abundant nitrogen isotope ^{14}N with spin quantum number $I = 1$ is often impractical because of the large quadrupolar couplings of the order of MHz and short relaxation time T_2.[15] Turning to the ^{15}N isotope, which has $I = 1/2$, its major disadvantage is the weak signal intensity caused by its low natural abundance of 0.37%. A few ^{15}N NMR studies of ^{15}N-labeled LC samples have been reported.[16,17] It was also recently demonstrated that natural abundance nitrogen-15 (NAN15) NMR spectra can be routinely recorded in static highly ordered samples of bulk LCs with strong anisotropic spin interactions.[18] Heteronuclear ^{13}C–^{15}N dipolar couplings can provide valuable information on short- and long-range structural parameters. With a carbon/nitrogen linewidth of the order of 10 Hz, the dipolar couplings for spin pairs separated by distances as large as 5 Å in thermotropic LCs with high molecular order can in principle be measured, thus providing structural and dynamic constraints over several chemical bonds. However, experimental detection of ^{13}C–^{15}N dipolar splittings at the natural abundance level is challenging because of the low fraction of 4×10^{-5} of naturally occurring ^{13}C–^{15}N coupled pairs. Thus, ^{13}C–^{15}N dipolar couplings were not exploited in studies of unlabeled LCs until very recently.[18,19] In a straightforward but long experiment on the 4-cyano-4′-pentylbiphenyl (5CB) nematic phase (88k scans over 48 h), ^{13}C satellites were observed in its NAN15 spectrum.[18] The measurement time required using this approach is impractically long for most applied studies. A further complication arises from the presence of the orders-of-magnitude stronger line from uncoupled ^{15}N spins in the spectrum. In another recent experiment performed in a weakly ordered ionic smectic A phase, small ^{13}C–^{15}N dipolar splittings in ^{13}C spectra were observed.[19] In more conventional thermotropic LCs with high molecular order, this experiment suffers from further sensitivity losses and longer measurement time because of the heating effects induced by radio-frequency (rf) irradiation with a high power required for efficient spin decoupling. The above considerations prompted us to explore new strategies and experimental designs to increase the signal intensity of ^{13}C–^{15}N pairs and suppress signals of uncoupled spins.

In the present study, we introduce new approaches to measure ^{13}C–^{15}N dipolar couplings in unlabeled LC samples. The proposed experiments are applied to highly ordered nematic LCs and enable measurements of coupling constants in a wide range of 10–1000 Hz with high sensitivity and spectral resolution. Spectra are recorded in static (non-rotating) samples with the phase director aligned in the magnetic field. Experimental data are compared with the results of density functional theory (DFT) and molecular dynamics (MD) computational analyses. We anticipate that the proposed pulse sequences for ^{13}C–^{15}N dipole spectroscopy will provide novel routes to characterize LC samples with natural isotopic abundance.

2. ^{13}C–^{15}N dipolar NMR spectroscopy

One faces several challenges when designing experimental techniques to measure ^{13}C–^{15}N dipolar coupling in LCs with natural isotope abundance, including the weak signal caused by the low abundance of isotopes, the strong signal of the central line due to uncoupled spins, rf heating effects, and field and temperature drifts during the long measurement time. A major challenge is to detect the very weak signal of the ^{13}C–^{15}N coupled pairs, which have a natural occurrence of only $\sim 4 \times 10^{-5}$, separately from the signals of uncoupled spins that are several orders of magnitude stronger. Indirect proton detection is commonly used in solution NMR spectroscopy[20] and also recently in solid-state magic angle spinning NMR spectroscopy[21] to increase the detection sensitivity of low-γ low-abundance nuclei. However, this technique is inefficient in LCs, where proton spectra of static samples typically consist of $\sim$10 kHz-wide unresolved lines. The sensitivity limit in practical detection is also constrained by the time available for a specific measurement. In this work, we broadly accept that an experiment is practically feasible if spectral lines of interest can be clearly observed above the noise level (typically, signal-to-noise ratio S/N > 3) after measurement overnight ($\sim$12 h) or for a shorter period.

2.1 ^{15}N detection

In this study, we use two approaches to measure ^{13}C–^{15}N dipolar couplings in LCs by recording ^{15}N spectra: the direct recording of NAN15 spectra and a new technique based on ^{13}C–^{15}N polarization transfer. Practical pulse sequences for the former and latter techniques are shown in Fig. 1a and b, respectively.

Straightforward accumulation of a large number of ^{15}N NMR transients, either after a single 90° pulse or using nuclear Overhauser effect (NOE) or cross-polarization (CP) enhancement, leads to a spectrum consisting of a strong central line and weak ^{13}C dipolar satellites with intensities of $\sim$1/180 of that of the central line. This technique is suitable to measure relatively large couplings (in the kHz range) when the satellite peaks and central line are sufficiently separated, as illustrated by the model spectrum in Fig. 1a. An advantage of this technique is that only a double-frequency probe is needed and standard heteronuclear pulse programs can be readily used. However, the measurement time can be impractically long, especially if no efficient nitrogen polarization enhancement from abundant protons by NOE or CP can be achieved.

We did not observe any significant ^{15}N NOE effect in LC samples studied in this and previous work.[18,19] Ramped Hartmann–Hahn CP (HH-CP) is commonly used to enhance ^{15}N polarization in samples with static dipolar couplings, such as LCs and solids. It has been shown that in static oriented samples of LCs, ^{13}C CP *via* adiabatic demagnetization in the rotating frame (ADRF-CP) leads to a higher signal gain than HH-CP.[22] We observed a similar advantage of ADFR-CP when recording ^{15}N spectra for the studied LC samples.

The second proposed ^{15}N-detecting experiment provided both higher spectral resolution and greater sensitivity than

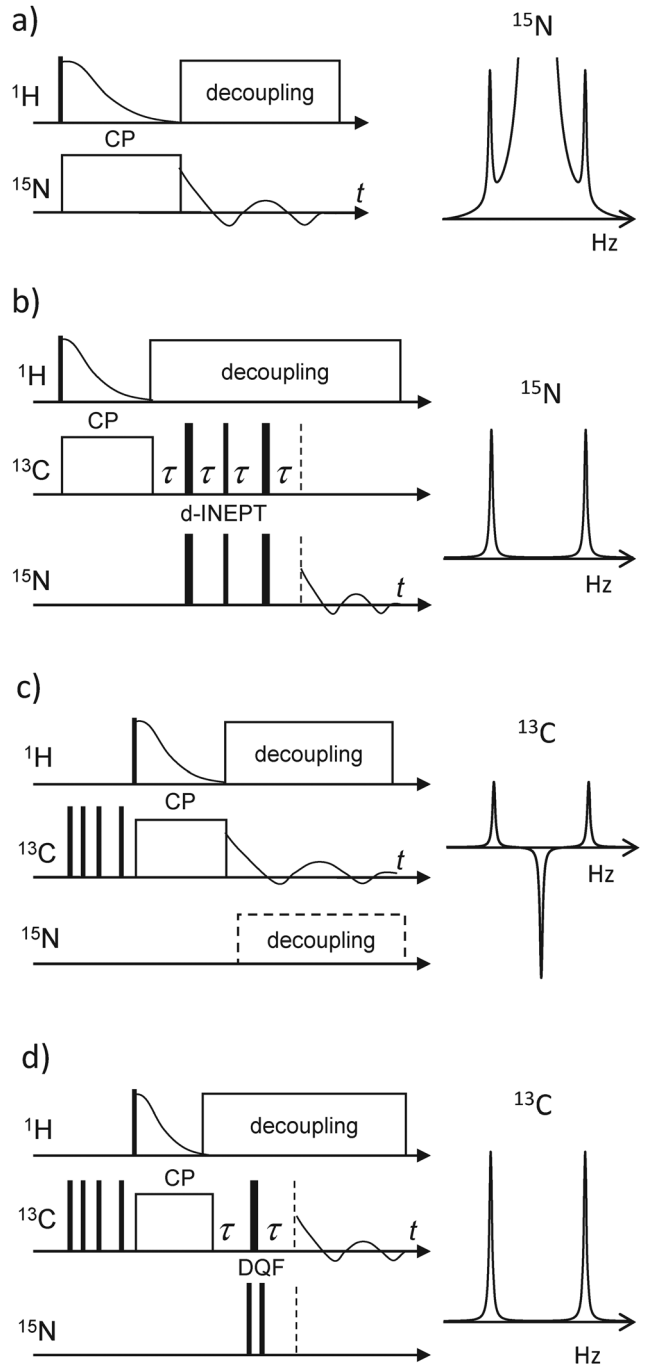

Fig. 1 Radiofrequency pulse sequences to measure ^{13}C–^{15}N dipolar coupling in (a and b) ^{15}N and (c and d) ^{13}C spectra of LC samples with natural isotopic abundance. In the right panel, model spectra are displayed. (a) Conventional NAN15 NMR using CP from protons. (b) ^{13}C–^{15}N dipolar INEPT. (c) ^{13}C difference spectroscopy: spectra acquired without and with nitrogen decoupling in alternating scans are subtracted. (d) Carbon-13 NMR with a heteronuclear ^{13}C–^{15}N double-quantum filter. All spectra are recorded in the presence of heteronuclear proton decoupling. Nitrogen or carbon spins are cross-polarized from protons using ADRF-CP. In carbon-detecting experiments, saturating 90-degree rf pulses are applied to destroy any initial carbon magnetization. For INEPT and DQF sequences, 16-step phase cycles of the rf pulses are used, as specified in ESI,† to select the ^{13}C–^{15}N coherences.

those of the first. This technique is based on INEPT (insensitive nuclei enhanced by polarization transfer[23]) coherence transfer using the ^{13}C–^{15}N dipolar interaction, as shown in Fig. 1b. The refocusing delay τ in the dipolar INEPT sequence (d-INEPT) is set to match the ^{13}C–^{15}N dipolar coupling magnitude $\tau = 1/(8D_{CN})$. The conventional phase cycle of the rf pulses in the INEPT transfer, as detailed in the ESI,† is applied to suppress signals of uncoupled ^{15}N spins. Proton heteronuclear dipolar decoupling is applied during d-INEPT delays to extend the ^{13}C and ^{15}N coherence lifetimes. With the central peak eliminated, doublets with small splitting can be resolved. In ^{13}C–^{15}N d-INEPT experiments, the intensity of the satellite signals is enhanced with a maximum theoretical factor of $\gamma_{^{13}C}/\gamma_{^{15}N}$. Furthermore, the carbon polarization is increased by HH- or ADFR-CP from protons.

2.2 ^{13}C detection

Because of the larger γ ratio of carbon-13 spins, ^{13}C spectra are expected to provide a higher sensitivity of the signal of ^{13}C–^{15}N pairs by a rough factor of $(\gamma_{^{13}C}/\gamma_{^{15}N})^{5/2}$ compared with that of ^{15}N spectra.[24] Despite the higher sensitivity of ^{13}C detection, we found that the straightforward recording of ^{15}N satellites in conventional carbon spectra is in practice more difficult compared with the analogous approach in ^{15}N spectra. The reasons for this are as follows. First, because of the 0.365% abundance of the ^{15}N isotope, the intensity of its satellite peaks is $\sim$1/550 of that for the main signal. This is three times smaller than the intensity of ^{13}C satellites in ^{15}N spectra; thus, the issue of the overlap with the central line is more severe. The second complication is a potential overlap with ^{13}C–^{13}C homonuclear dipolar doublets, which are three times more intense than ^{13}C–^{15}N ones. Therefore, the experimental approaches described below were designed to eliminate spectral peaks caused by ^{13}C spins not coupled with ^{15}N.

In the experiment using the sequence shown in Fig. 1c, ^{13}C CP spectra acquired without and with ^{15}N decoupling in alternate scans are subtracted from each other. In the resulting difference spectrum, the central peak of uncoupled spins is suppressed while preserving the signal of ^{13}C–^{15}N coupled pairs. A strong dipolar interaction (of >kHz range) with abundant ^{1}H spins is removed by high-power proton decoupling applied to both spectra. In the scans acquired without nitrogen decoupling, the ^{13}C–^{15}N coupled pairs lead to dipolar doublets in the ^{13}C spectrum, whereas they contribute to a residual central peak in the scans with ^{15}N decoupling. The difference spectrum thus represents a superposition of the ^{13}C–^{15}N doublet and the central peak of the opposite sign (Fig. 1c). In this experiment, it was possible to observe even small splittings giving rise to satellites close to the central frequency. In practice, to balance rf heating effects, ^{15}N irradiation was also applied in the scans without decoupling under off-resonance conditions, effectively leading to no decoupling.

The central peak is of the opposite sign and twice as intense as the satellites. The overlap with the central negative line can compromise the resolution and peak intensity of small splittings comparable to the linewidth. The central peak can be

suppressed by matching the relative numbers of scans with and without decoupling to the natural abundance level of ^{15}N of 0.365%. Considering that 1–0.00365 is $\sim$272/273, in the difference spectrum of 273 transients recorded without ^{15}N decoupling and 272 scans with decoupling, the central peak is suppressed to a level $<$1% of the satellite intensity. In such a difference spectrum with a compensating scan, both the signal intensity and resolution are improved because of the less severe effect of the spectral overlap, as demonstrated by numerical analysis (see the ESI†). This approach is also robust with respect to spectral artifacts caused by temperature or field drifts.

In the second proposed ^{13}C-detecting experiment illustrated in Fig. 1d, signals of carbon spins coupled to ^{15}N are selected using a heteronuclear double quantum filter (DQF).[20] The strong central peaks from uncoupled ^{13}C spins as well as ^{13}C–^{13}C satellites are rejected after two basic phase cycles of rf pulses. During delays τ, coupling to protons is suppressed by heteronuclear decoupling, while the ^{13}C chemical shift is refocused. Therefore, carbon spin evolution is solely determined by the heteronuclear coupling to ^{15}N. DQF coherence is selected using the phase cycle given in the ESI.† The τ value is optimized for the range of the dipolar coupling values to be measured. To increase carbon polarization, ADRF-CP from protons is used. Pre-saturation 90° ^{13}C pulses suppress the signal due to direct carbon magnetization. For carbon sites where CP is inefficient, ^{13}C 90° single pulse excitation (SPE) or NOE enhancement can be used.

3. Experimental

Nematic LC samples of 4-methoxybenzylidene-4′-butylaniline (MBBA, CAS No. 26227-73-6) and 4,4′-bis(butylamino)biphenyl (BAB, CAS No. 5324-31-2) were obtained from Sigma Aldrich and Angene International, respectively, and were used as received. The following phase transition temperatures were observed: MBBA isotropic $\xrightarrow{+45\,^{\circ}C}$ nematic $\xrightarrow{+20\,^{\circ}C}$ crystal, BAB isotropic $\xrightarrow{+96\,^{\circ}C}$ nematic $\xrightarrow{+72\,^{\circ}C}$ crystal.[25] Samples (0.5 ml) were loaded in standard 5 mm NMR tubes. In the nematic phase, the sample director is homogeneously aligned parallel to the magnetic field of the NMR magnet.

Experiments were performed using a Bruker 500 Avance III spectrometer at Larmor frequencies of 500.1, 125.7, and 50.7 MHz for ^{1}H, ^{13}C, and ^{15}N, respectively. A solution state triple-frequency probe ^{1}H–^{15}N–BBO (broadband observe probe) was used. The ^{1}H, ^{13}C, and ^{15}N pulse lengths were 7, 15 and 30 μs, respectively. The ^{15}N chemical shift was referenced relative to liquid NH_3 by using the ^{15}N resonance at 77 ppm of 0.1 M urea solution in DMSO as an external reference.[26]

For heteronuclear proton decoupling in the ^{13}C and ^{15}N spectra, the spinal64 sequence[27] with a nutation frequency of 20 and 10 kHz, respectively, was applied. For heteronuclear ^{15}N decoupling in the ^{13}C spectra, the spinal64 sequence with a nutation frequency of 2.5 kHz was used. In the difference spectrum, the decoupler carrier frequency was shifted 10 kHz off-resonance in the scans without ^{15}N decoupling. The heteronuclear decoupling sequences were applied in synchronized mode, when the decoupling cycles were always initiated at the same point of the pulse sequence. ADRF-CP with a half-Gaussian pulse on the proton channel was used for ^{13}C and ^{15}N signal enhancement. Contact times were optimized in the range 5–10 ms and nutation frequencies were in the range 5–15 kHz. The number of scans and relaxation delays are specified in figure captions. Phase cycles of the rf pulses in the pulse sequences are given in the ESI.†

4. Results

4.1 ^{15}N spectra

In aligned LC samples, large dipolar ^{13}C–^{15}N couplings of the order of kHz can be directly observed in ^{15}N NMR spectra. The first NAN15 spectrum with ^{13}C dipolar satellites was recently measured in nematic 5CB.[18] However, the experiment required about 2 days of instrumental time to accumulate a sufficient number of scans.

The NMR signal intensity in LCs can be increased by CP transfer from protons. The ADRF-CP ^{15}N spectrum of nematic MBBA is displayed in Fig. 2a. CP parameters were optimized for low rf field magnitudes ($\sim$8 kHz) to minimize rf heating effects. An experimental enhancement factor of 4.7 was obtained, which is higher than that of 3.6 using ramped HH-CP. This spectrum required 18 h of experimental time to accumulate 16k scans with a recycling delay of 4 s. The spectrum contains a dipolar doublet with 1.3 kHz splitting. The splitting is assigned to the coupling to the directly bonded carbon C1 (for coupling assignment, see ^{13}C spectra below). The intensity of the doublet peaks relative to the central line is $\sim$1/180, which is in accordance with the ^{13}C abundance of 1.1%. The achieved S/N ratio for the doublet peaks is $\sim$3.2. Because dipolar spectra are intrinsically symmetric, spectrum symmetrization by reversing the spectrum and adding it to itself can be applied to further improve S/N by a factor of $2^{1/2}$; this procedure was not applied to the spectra in Fig. 2.

Smaller couplings to remote carbons cannot be resolved in the spectrum in Fig. 2a because of the overlap with the central line. In d-INEPT spectra, the central line is suppressed (Fig. 2b and c). Using a short delay τ of 150 μs in the d-INEPT sequence optimized for the strong coupling to aromatic carbon C1, a doublet with a large splitting matching that in the spectrum in Fig. 2a is observed. The estimated intensity gain due to combined effects of ^{1}H–^{13}C ADRF-CP and ^{13}C–^{15}N d-INEPT is $\sim$7.0 and the obtained S/N is 4.8. Because CP enhancement of the carbon C1 in the ^{13}C CP spectrum was found to be 2.8, the INEPT enhancement is calculated to be 7.0/2.8 = 2.5, corresponding to a transfer efficiency of almost 100%.

In the experiments with the d-INEPT filter, it is also possible to record dipolar doublets originating from weaker couplings to remote carbons. Satellites caused by remote ^{13}C spins were observed by matching delay τ to small coupling values. The resolved doublet with a splitting of 200 Hz, as seen in Fig. 2c, was assigned to coupling to carbon C1′. Some other expected smaller splittings were not resolved in this experiment.

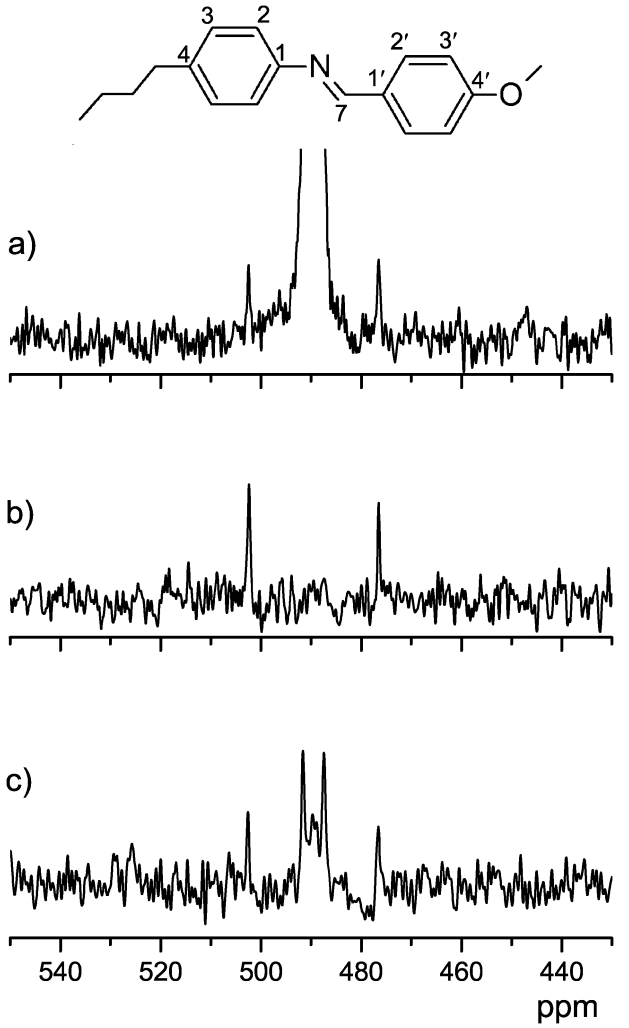

Fig. 2 The ^{15}N NMR spectra of MBBA in the nematic phase at 20 °C. (a) ADRF-CP ^{15}N spectrum. (b and c) d-INEPT ^{13}C–^{15}N spectra obtained using the pulse sequence of Fig. 1b, with delay τ = 150 and 1000 μs, respectively. For each spectrum, 16k scans were accumulated with a relaxation delay of 4 s (18 h measurement time).

4.2 ^{13}C spectra

Recently, we showed that ^{13}C difference spectra obtained by the sequence depicted in Fig. 1c in a weakly ordered smectic mesophase of an ionic liquid can reveal satellites caused by carbon–nitrogen combined dipolar and *J*-couplings of the order of 100 Hz and smaller.[19] Here, we extend this approach to thermotropic LCs with a high molecular order parameter S of >0.5 and corresponding strong dipolar interactions up to the kHz range.

A BAB sample exhibiting a high-temperature nematic phase has the advantage of containing two equivalent nitrogen atoms in its molecular structure, which improves the sensitivity of NMR spectra (Fig. 3). The location of the nitrogen atoms in the linkage between the rigid biphenyl core and flexible butyl chains provides the opportunity to study the influences of both structural and dynamic parameters on dipolar interactions.

Fig. 3a depicts a conventional ^{13}C CP spectrum of nematic BAB. To minimize rf heating in this temperature-sensitive sample,

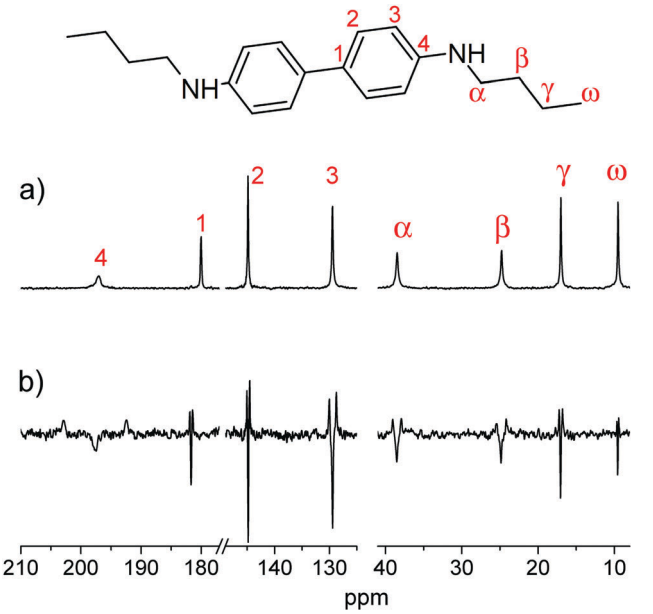

Fig. 3 The carbon-13 spectra of nematic BAB at 73 °C. (a) Single scan conventional proton-decoupled carbon-13 CP spectrum. (b) ^{13}C difference spectrum acquired with nitrogen-15 decoupling in alternating scans. The aromatic (left) and aliphatic parts (right) were collected in separate experiments. For the difference spectra, 8k scans were accumulated with a relaxation delay of 4 s (9 h measurement time).

the proton decoupling field was limited to 20 kHz and the signals of the aromatic and aliphatic carbons were acquired in separate experiments with individually optimized proton decoupling frequency offsets.

The ^{13}C difference spectrum with scan-alternated ^{15}N decoupling in Fig. 3b displays a number of ^{13}C–^{15}N dipolar doublets (positive peaks) and ^{13}C central lines (negative peaks). The couplings to ^{15}N for all inequivalent carbon atoms in the molecule, including those in butyl chains, are observed. Remarkably, couplings of the spins separated by up to four chemical bonds and by distances as large as 5 Å are resolved. For the rigid biphenyl fragment, the coupling values are consistent with the core geometry, as detailed in Section 5 below. In the aliphatic chain, the coupling constant for the β carbon exceeds that for the directly bonded α carbon. This is a consequence of the tilt of the internuclear vector N–Cα relative to the main molecular rotation axis at angle close to the magic angle of $\sim 55^\circ$.

We also recorded ^{13}C difference spectra for MBBA and compared the ^{13}C–^{15}N splittings with those observed in the ^{15}N-detecting experiment. Fig. 4a shows a single-scan ^{13}C ADRF-CP spectrum of the aromatic chemical shift range for MBBA. The enhancement factor compared with an SPE spectrum is between 3 and 5 for different peaks. The broadening and low intensity of the signal from carbon C1 is attributed to the strong dipolar coupling to the fast-relaxing quadrupolar ^{14}N nucleus.

A ^{13}C difference spectrum with scan-alternated ^{15}N decoupling was acquired using the sequence in Fig. 1c with suppression of the central peaks by adding a compensating scan. The compensating scan indeed resulted in elimination of the residual

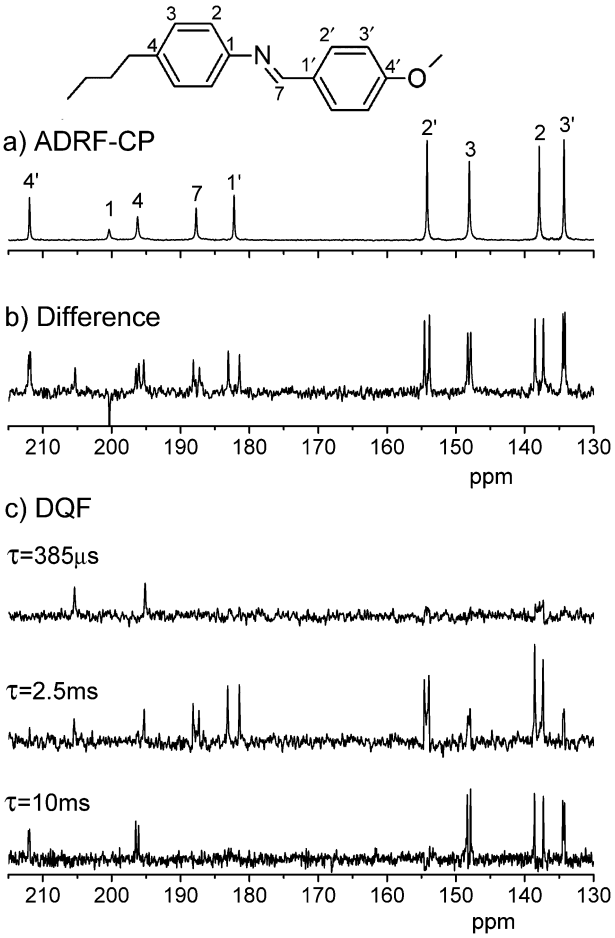

Fig. 4 The carbon-13 spectra in nematic MBBA at 20 °C. (a) Single scan conventional proton-decoupled carbon-13 CP spectrum. (b) ^{13}C difference spectrum acquired with nitrogen-15 decoupling in alternating scans and with a compensating scan using the pulse sequence of Fig. 1c. 4360 scans were accumulated with a relaxation delay of 9 s (11 h measurement time). (c) DQF ^{13}C–^{15}N dipolar spectra recorded using the sequence of Fig. 1d at indicated delays τ. 2k scans were accumulated with a relaxation delay of 9 s (5 h measurement time).

negative line for most carbons. All the carbons in the molecular core exhibited resolved dipolar splittings because of coupling to ^{15}N. The largest observed splitting of 1.32 kHz is for the C1 carbon directly bonded to nitrogen. The coupling of imine carbon C7, despite being the closest to nitrogen, is relatively small because the C=N bond angle relative to the molecular rotational axis is in the vicinity of the magic angle (see the MD analysis below). Quite remarkably, small coupling to the distant carbon C4′ (~5 Å) in the phenyl ring was also observed. Comparing ^{15}N and ^{13}C spectra, one can assign the two largest splittings of 1320 and 200 Hz in the ^{15}N spectra in Fig. 2 to carbons C1 and C1′, respectively.

DQF ^{13}C–^{15}N dipolar spectra of nematic MBBA recorded using the sequence in Fig. 1d with different delays τ are compared in Fig. 4c. The sensitivity of the DQF experiment is superior to that of the difference experiment. Each spectrum in Fig. 2c required only 2k scans and an experimental time of 5 h for this sample with natural isotopic abundance. The carbon polarization gain provided by ADFR-CP is essential to record spectra of LCs within an experimental time of only a few hours.

With a relatively short delay τ of 385 μs in the DQF step, the C1 carbon signal is observed giving rise to a doublet with a splitting of 1.32 kHz. Spectra recorded with longer τ values exhibit a number of doublets with smaller splittings. The couplings are consistent with those in the spectrum of Fig. 4b obtained by the difference method. The smallest resolved splitting of 20 Hz originates from carbon 4′, which is separated from nitrogen by five chemical bonds and a distance of about 5 Å.

5. Discussion

5.1 Comparison of experimental methods

The presented spectra demonstrate the feasibility of experimental studies of direct through-space ^{13}C–^{15}N spin couplings in highly ordered LC phases without isotopic enrichment. In conventional NAN15 spectra, the ^{13}C–^{15}N dipolar splittings are observed as weak ^{13}C satellites around the ^{15}N line. This approach is instrumentally and methodologically the least demanding of those considered here but requires a very long measurement time. Application of efficient polarization enhancement techniques, such as HH-CP or ADRF-CP, where the latter provides higher sensitivity for static LCs than the former, is essential. Because only a double-frequency ^{15}N/^{1}H probe is needed, the experiment can be carried out on most high-resolution NMR spectrometers. However, the technique is limited to recording relatively large couplings (kHz range) when the doublet peaks are well separated from the central line, which is orders of magnitude more intense than the doublets, as exemplified by the spectrum in Fig. 2a.

To access smaller splittings, the central line caused by uncoupled spins must be suppressed. In the ^{15}N detection approach, this is achieved using the ^{13}C–^{15}N d-INEPT technique. The two-step phase cycle cancels out the central peak to reveal both large and small splittings (Fig. 2b and c). We also observed higher ^{15}N signal enhancement with two combined polarization transfer steps, ^{1}H–^{13}C CP and ^{13}C–^{15}N INEPT, compared with the case of direct ^{1}H–^{15}N CP. This was attributed to the stronger ^{1}H–^{13}C dipolar couplings than the ^{1}H–^{15}N ones, which facilitate more efficient CP dynamics that competes with spin relaxation. The triple-frequency ^{15}N d-INEPT experiment required hardware with three frequency channels and a ^{15}N/^{13}C/^{1}H probe.

While we demonstrated the feasibility of the ^{15}N detection technique, the signal sensitivity was noticeably inferior to that of ^{13}C detection methods. In the ^{13}C detection technique, the expected theoretical sensitivity gain is $(\gamma_C/\gamma_N)^{5/2} \approx 10$, assuming similar linewidths for ^{13}C and ^{15}N resonances.[24] In practice, the observed sensitivity of the ^{13}C DQF method is four to five times higher than that of ^{15}N INEPT when comparing the spectra in Fig. 4 and 2, respectively (accounting for the numbers of added scans). The splitting assignment in the ^{13}C spectra was also straightforward. In the case of more than one nitrogen atom present in a molecule, selective nitrogen decoupling can be used.[19]

Resonances from carbons in molecules not containing the ^{15}N isotope (constituting 99.6% of a sample) were efficiently suppressed below the noise level by ^{13}C–^{15}N DQF with a conventional 16-step phase cycle (listed in the ESI†). The optimal delay τ in the DQF sequence depends on the magnitude d of the spin coupling constant, $\tau = 1/4d$, which provides in-phase doublet peaks of maximal intensity. Therefore, to measure dipolar couplings over a broad range, as for the MBBA sample in Fig. 4, it is necessary to perform several experiments with different τ delays. The magnitude-mode Fourier transform, rather than phase-sensitive mode, is preferred to accurately determine dipolar couplings from the experimental splittings in DQF ^{13}C spectra because this removes phase distortion, as demonstrated in the ESI.†

The star-like coupling network between a ^{15}N spin and many surrounding ^{13}C spins can provide complementary structural information that is not available from more conventional block-wise networks like ^{13}C–^{1}H couplings. The experimental time for a 1D ^{13}C–^{15}N experiment is in fact comparable to that for a typical 2D ^{13}C–^{1}H SLF experiment. In addition, ^{13}C DQF experiments can be also performed in a 2D mode by incrementing the delay between nitrogen 90° pulses in Fig. 1d, analogous to the solution-state *J*-coupling-based Heteronuclear Multiple Quantum Coherence (HMQC) technique. Spreading the ^{15}N signals in the second dimension can be useful in the case of multiple nitrogen atoms in a molecule. However, the measurement time for a 2D experiment in isotopically unlabeled samples would be prohibitively long with our present set-up.

The ^{13}C detection approach with scan-alternated ^{15}N decoupling (the sequence in Fig. 1c) has been previously applied to a weakly ordered ionic mesophase with relatively small splittings of ~100 Hz.[19] Application of this technique to conventional highly ordered thermotropic LCs with kHz-range ^{13}C–^{15}N dipolar interactions, such as MBBA, is demonstrated here for the first time. Spin decoupling of low-γ ^{15}N nuclei requires a decoupling field with a large amplitude $B_1 = 2\pi\nu_{rf}/\gamma_N$ with a nutation frequency exceeding the dipolar coupling magnitude $\nu_{rf} > D_{CN}$. Nitrogen decoupling in combination with simultaneous proton decoupling induces a considerable temperature increase and gradients in LC samples. Because the ^{13}C anisotropic chemical shift in LCs is highly sensitive to temperature, the rf heating caused by spin decoupling leads to line broadening and associated intensity and resolution losses. In MBBA and BAB samples, the rf heating was minimized by optimizing decoupling parameters at limited rf power and by extending recycling delays. With these precautions, ^{13}C–^{15}N dipolar spectra with a resolution comparable with that of DQF spectra were obtained. In contrast to the DQF experiments, the difference technique with ^{15}N decoupling is non-selective with respect to the coupling magnitude. Thus, all resolved splittings can be observed with comparable sensitivity in a single experiment.

A drawback of the difference approach is that every other scan contains no useful signal (dipole doublet). Therefore, the S/N halves compared with that of the DQF method. The negative central lines present in the difference spectra decrease the resolution and intensity of doublets with small couplings because of partial cancellations of the overlapping negative and positive peaks. This issue can be mitigated by adding a compensating scan to suppress the central line, as demonstrated in the ESI.† The compensating scan approach assumes that the ^{13}C line broadening caused by dipole coupling to fast-relaxing ^{14}N spins is negligible. Fortunately, such broadening is only considerable for strongly coupled spins, which exhibit no overlap, as exemplified by the signal of the C1 carbon in the spectrum in Fig. 4b.

In the studied samples, the ^{13}C–^{15}N couplings for directly bonded atoms as well as for atoms separated by several chemical bonds and distances of up to 5 Å were measured. Single-bond dipolar couplings in LCs, most commonly for CH bonds, are often used to calculate bond order parameters to characterize molecular dynamics.[3] In contrast, a star-like coupling network between remote spins provides useful information about structural and dynamic constraints in flexible molecules.[9,28,29] Resolving couplings over distances of up to 5 Å is a rather remarkable result considering that both involved isotopes have relatively low γ ratios and that the couplings are partly averaged by anisotropic molecular dynamics. Unlike when measuring couplings to abundant spins, such as protons, no homonuclear decoupling is needed. Therefore, a complication in SLF spectroscopy caused by the uncertainty of the coupling scaling by homonuclear decoupling is avoided.[3]

5.2 Comparison of experimental and computational results

Anisotropic molecular mobility in mesophases leads to a partial averaging of spin interactions. The averaging is over rotations around the long molecular axis, fluctuations of the molecular axis around the director, and the conformational transitions in flexible molecular parts. Intermolecular spin interactions, such as dipolar couplings, are typically averaged to zero by molecular translational diffusion.[30]

Dipolar couplings in LCs are interpreted in terms of the second-rank molecular order parameter tensor *S*. For a nematic phase aligned along the magnetic field $\boldsymbol{B}_0$, the partly averaged nitrogen–carbon dipolar coupling constant is given by[31,32]

$$\langle D_{CN}\rangle = -\frac{\mu_0}{8\pi^2}\gamma_C\gamma_N\hbar\left[S_{ZZ}\left\langle\frac{3\cos^2\theta_{CN,Z}-1}{2r_{CN}{}^3}\right\rangle + (S_{XX}-S_{YY})\left\langle\frac{\cos^2\theta_{CN,X}-\cos^2\theta_{CN,Y}}{2r_{CN}{}^3}\right\rangle\right] \quad (1)$$

where $\theta_{CN,\alpha}$ is the angle between the C–N vector (defining the interaction frame) and the axes $\alpha = X, Y, Z$ of a molecular frame where the order parameter matrix is diagonal. S_{ZZ} and $S_{XX} - S_{YY}$ are the molecular orientational order and biaxiality parameter, respectively. $S_{XX} - S_{YY}$ is small in nematic phases of molecules with high structural symmetry and fast internal rotations; that is, $S_{XX} - S_{YY} \ll S_{ZZ}$. For a rigid molecule, $b_{CN} = -(\mu_0/8\pi^2)(\gamma_C\gamma_N\hbar/r_{CN}{}^3)$ is the coupling constant in the interaction principal axis frame.

The observed experimental splittings $\Delta\nu = |2D_{CN} + J_{CN}|$ are determined by the combined effects of the residual direct dipole–dipole heteronuclear interaction D_{CN} and indirect scalar coupling J_{CN}, the anisotropy of which is usually small compared

with dipolar coupling values and can be neglected.[32] The values for one-bond and two-bond J_{CN} couplings are $\sim$10 and $\sim$5 Hz, respectively. Therefore, in the samples studied here, the dominant contribution to the observed splittings is the dipolar interaction. Below, we compare the experimentally determined ^{13}C–^{15}N coupling constants for BAB and MBBA with those estimated from molecular geometries calculated by DFT analysis and MD simulations, respectively.

5.2.1 Comparison with DFT data for BAB. Distances r_{CN} and angles θ_{CN} in BAB were calculated from the equilibrium molecular geometry obtained by the DFT B3LYP/6-311+g(d) method[33] and are presented in the ESI.† Based on the structural symmetry and rapid internal molecular rotations in nematic BAB, we assume that (i) $S_{XX} - S_{YY}$ is small ($S_{XX} - S_{YY} \ll S_{ZZ}$) and (ii) the principal order axis coincides with the long molecular axis, which is also close to the axis of the biphenyl fragment. The S_{ZZ} value of BAB has not been reported in the literature, to the best of our knowledge. One can estimate S_{ZZ} most accurately from the experimental dipolar coupling in the directly bonded pair C4–N with $\theta_{CN,Z} \approx 0$ using the relationship $D_{CN} \approx b_{CN}S_{ZZ}(3\cos^2\theta_{CN,Z} - 1)/2 \approx b_{CN}S_{ZZ}$. The obtained S_{ZZ} value is then applied as a scaling factor to other C–N coupling constants derived from the DFT-optimized molecular geometry.

Within the described model, using experimental value D_{CN} = 660 Hz for the C4 carbon and the bond distance of 1.39 Å obtained from the DFT analysis, the calculated order parameter SZZ is 0.58. Based on the molecular geometry parameters (given in the ESI†) and using this S_{ZZ} value, the calculated magnitudes of D_{CN} for the other carbons in the adjacent phenyl ring C1, C2, and C3 are 23, 29, and 78 Hz, respectively. These numbers are in good agreement with the experimental values D_{CN}^{exp} estimated as half of experimental splittings in the spectrum of Fig. 3b (Table 1).

Similar analysis for the carbons in the flexible dynamically disordered aliphatic chain of BAB was not straightforward. However, an estimation can be made for Cα, because the C1–N–Cα bond angle is not strongly affected by the conformational dynamics of BAB. Based on the small experimental coupling of 70 Hz for this directly bonded Cα–N pair compared with the principal frame dipolar constant of b_{CN} = −1005 Hz, we were able to conclude that the bond angle relative to the molecular rotation axis is in the vicinity of the magic angle ($\sim$55°). Indeed, DFT analysis predicted that $\theta_{CN,Z}$ = 57° for this pair. The disparity between predicted and experimental couplings for Cα (Table 1) is caused by the high sensitivity of the prediction to the precise value of $\theta_{CN,Z}$ approaching the magic angle.

Table 1 Comparison of experimental D_{CN}^{exp} and calculated D_{CN} ^{13}C–^{15}N coupling magnitudes (Hz) in BAB

Carbon	$\lvert D_{CN}\rvert$	$\lvert D_{CN}^{exp}\rvert$
C4	660	660
C3	78.0	80
C2	29.3	32
C1	23.2	24
Cα	32.0	70
Cβ	96.5	75
Cγ	17.5	27
Cω	11.4	12

For other carbons in the chain, average couplings are influenced by the conformer probability distributions[34] and thus are not readily comparable to DFT data for the molecule with extended all-trans chains. Some estimations for the Cβ and Cγ couplings can be made considering a *trans–gauche* isomerisation model of the butyl chains. A conformation transition about the N–Cα bond does not affect the Cβ–N atomic distance. However, due to a change of the angular factor the coupling constant for gauche conformers decreases to $\approx$40 Hz. Thus, it is reasonable to expect a smaller average value of the Cβ–N coupling in the presence of chain dynamics, in agreement with the experimental observation (Table 1). Similar analysis can be applied to the Cγ carbon. Here, the larger value of the experimental coupling compared to the calculated one is due to the contribution of gauche conformers exhibiting a shorter Cγ–N distance than that in all-trans chains.

5.2.2 Comparison with MD data for MBBA. Molecular structure, conformational dynamics, and local orientational ordering in the MBBA nematic phase have been previously studied by computational modeling using MD methods. Details of the computer simulation and the parameters of the force fields were reported in a previous publication[35] and are presented in the ESI.† Trajectories generated in computer simulations contain comprehensive information about the microscopic parameters of molecules in a mesophase. Having access to the coordinates for all atoms in a trajectory makes it possible to calculate order parameter values and dipolar interaction constants.

The S_{ZZ} value calculated from the trajectory is 0.664. This value is larger than typical values reported in the literature for MBBA in the relevant temperature range, as discussed in the ESI.† Since S_{ZZ} is a sensitive function of $\Delta T = T - T_c$ (T is the temperature in the nematic phase and T_c is the temperature of the nematic-to-isotropic transition), the larger MD-derived S_{ZZ} value than the experimental one may be a consequence of an inconsistent temperature shift ΔT. Because the nematic-to-isotropic transition was not tested in the MD simulation, the trajectory temperature cannot be properly referenced to T_c. The higher order parameter S_{ZZ} obtained in MD analysis leads to an overestimation of the dipolar couplings which are proportional to S_{ZZ} (if neglecting the contribution of the small biaxiality term in eqn (1)).

Fortunately, the experimental S_{ZZ} in our MBBA sample can be estimated from the anisotropic contribution $\Delta\delta = \delta_{nem} - \delta_{iso}$ to the ^{13}C chemical shifts of phenyl ring carbons using the semi-empirical relationship $S_{ZZ} = \alpha\Delta\delta + \beta$. Using the reported values of the parameters α and β for an MBBA homologous series,[36] the consistent value $S_{ZZ} = 0.56 \pm 0.01$ is obtained for eight inequivalent carbons in the phenyl rings (details of the analysis are included in the ESI†). This value is also well within the reported experimental range. Thus, to account for the discrepancy of the modeling and experimental values of S_{ZZ}, the couplings obtained from the MD trajectory are scaled

Table 2 Comparison of experimental D_{CN}^{exp}, obtained by different methods, and theoretical dipolar couplings D_{CN} (Hz) in MBBA

Carbon	MD values $0.85\|D_{CN}\|$	Experimental values $\|D_{CN}^{exp}\|^a$	$\|D_{CN}^{exp}\|^b$	$\|D_{CN}^{exp}\|^c$
C1	694	647	639	656
C2	78	81	79	
C3	29	30	29	
C4	24	27	27	
C7	90	59	57	
C1′	108	106	104	105
C2′	46	48	46	
C3′	17	18	18	
C4′	13	13	13	

[a] ^{13}C DQF spectra in Fig. 4c. [b] ^{13}C difference spectrum in Fig. 4b. [c] ^{15}N d-INEPT spectra in Fig. 2b and c.

by the factor $S_{ZZ}^{exp}/S_{ZZ}^{MD} \approx 0.85$. The scaling procedure allows for direct comparison of simulated and experimental data at similar order parameters under the assumption that the conformational distribution is not strongly affected by ΔT. Essentially, scaled MD data correspond to the LC sample at another temperature with a lower value of S_{ZZ}.

The MD-derived couplings $\langle D_{CN} \rangle$ obtained from eqn (1) as well as related distances and angles are presented in the ESI.† The magnitudes of the scaled theoretical couplings are compared with experimental values in Table 2. Experimental couplings are estimated as half of the splittings in the spectra of Fig. 2 and 4. Good agreement within experimental error between sets of couplings is found for most of the spin pairs. The exception is the pair N–C7, which exhibits high sensitivity to the precise value of the bond angle relative to the molecular rotational axis approaching the magic angle (see Table S2 in the ESI,† and also compare with the N–Cα coupling in BAB discussed above).

6. Conclusions

We developed and compared various experimental strategies to measure short- and long-range heteronuclear ^{13}C–^{15}N dipolar couplings in highly ordered LC samples with natural isotopic abundance. New techniques to record ^{13}C and ^{15}N NMR spectra of ^{13}C–^{15}N spin pairs, which have a natural abundance level of only 0.004%, with increased signal intensity and spectral resolution and suppression of the signals of the uncoupled isotopes were designed. The maximum sensitivity gain was obtained using a ^{13}C detection scheme with a ^{15}N double quantum filter and ADRF-CP transfer from protons. The coupling assignment was also straightforward for ^{13}C spectra, because the dipolar doublets are separated according to carbon chemical shifts. Spectra for samples with natural abundance of the two rare isotopes were acquired within an experimental time of a few hours. Couplings between spins separated by up to five chemical bonds and distances of up to 5 Å were measured. Because of the relatively low demands on rf power levels, the experiments were easy to implement using conventional high-resolution solution-state probes.

In the present study, couplings were obtained from the directly observed splittings in 1D spectra. For molecules with multiple inequivalent nitrogen atoms, it may be necessary to combine the new methods with a 2D technique, which however demands higher signal intensity. Further solutions to increase the sensitivity can be based on already available technological developments such as cryoprobes and stronger NMR magnets (B_0 of ∼20 T).

Direct dipolar spin couplings are among the most informative and sensitive probes for a wide range of dynamic processes and structural properties of LCs at the molecular and supramolecular level. The presented experimental methods to characterize the dipolar couplings in unlabeled materials provide novel routes to investigate the molecular structure and dynamics in LCs. The potential of these methods has been demonstrated here for highly ordered nematic phases of calamitic molecules, but measurements can be performed for many other kinds of ordered fluids. Because the developed techniques are applied to materials with natural isotopic levels, synthetically demanding and expensive isotopic labeling is avoided. We expect that these methods will become widely used in fundamental studies of various anisotropic mesophases.

Conflicts of interest

There are no conflicts to declare.

Acknowledgements

This work was supported by the Swedish Research Council VR grant 2017-04278 and by the RFBR grant 17-03-00057.

References

1 R. Y. Dong, *Nuclear Magnetic Resonance Spectroscopy of Liquid Crystals*, Worlds Scientific, London, 2010.
2 *Handbook of Liquid Crystals*, ed. J. W. Goodby, P. J. Collings, T. Kato, C. Tschierske, H. Gleeson and P. Raynes, Wiley, 2014.
3 S. V. Dvinskikh, in *Modern Methods in Solid-State NMR: A practitioners'Guide*, ed. P. Hodgkinson, Royal Society of Chemistry, Abingdon, 2018.
4 R. K. Hester, J. L. Ackerman, B. L. Neff and J. S. Waugh, *Phys. Rev. Lett.*, 1976, **36**, 1081–1083.
5 S. Caldarelli, in *Encyclopedia of Nuclear Magnetic Resonance*, ed. D. M. Grant and R. K. Harris, Wiley, Chichester, 2002, pp. 291–298.
6 C. Tan, C. Canlet and B. M. Fung, *Liq. Cryst.*, 2003, **30**, 611–615.
7 C. Canlet and B. M. Fung, *Liq. Cryst.*, 2001, **28**, 1863–1872.
8 C. Canlet and B. M. Fung, *J. Phys. Chem. B*, 2000, **104**, 6181–6185.
9 B. B. Kharkov, V. I. Chizhik and S. V. Dvinskikh, *J. Chem. Phys.*, 2012, **137**, 234902.

10 S. V. Dvinskikh, D. Sandström, H. Zimmermann and A. Maliniak, *Chem. Phys. Lett.*, 2003, **382**, 410–417.
11 S. V. Dvinskikh, D. Sandström, Z. Luz, H. Zimmermann and A. Maliniak, *J. Chem. Phys.*, 2003, **119**, 413–422.
12 H. Zimmermann, *Liq. Cryst.*, 1989, **4**, 591–618.
13 P. Lesot and O. Lafon, *Anal. Chem.*, 2012, **84**, 4569–4573.
14 M. E. Neubert, in *Liquid crystals: experimental study of physical properties and phase transitions*, ed. S. Kumar, Cambridge University press, Cambridge, 2001.
15 M. Witanowski and G. A. Webb, *Nitrogen NMR*, Plenum Press, London, 1973.
16 A. Höhener, L. Müller and R. R. Ernst, *Mol. Phys.*, 1979, **38**, 909–922.
17 A. P. Manning, M. Giese, A. S. Terpstra, M. J. MacLachlan, W. Y. Hamad, R. Y. Dong and C. A. Michal, *Magn. Reson. Chem.*, 2014, **52**, 532–539.
18 L. Jackalin and S. V. Dvinskikh, *Z. Phys. Chem.*, 2017, **231**, 795–808.
19 M. Cifelli, V. Domenici, V. I. Chizhik and S. V. Dvinskikh, *Appl. Magn. Reson.*, 2018, **4**, 553–562.
20 S. Berger and S. Braun, *200 and More NMR Experiments: A Practical Course*, Wiley, 2004.
21 T. Kobayashi, Y. Nishiyama and M. Pruski, in *Modern Methods in Solid-State NMR: A practitioners'Guide*, ed. P. Hodgkinson, Royal Society of Chemistry, Abingdon, 2018.
22 J. S. Lee and A. K. Khitrin, *J. Chem. Phys.*, 2008, **128**, 114504.
23 G. A. Morris and R. Freeman, *J. Am. Chem. Soc.*, 1979, **101**, 760–762.
24 M. H. Levitt, *Spin Dynamics*, Wiley, Chichester, 2001.
25 D. Demus and H. Zaschke, *Flüssige Kristalle in Tabellen II*, VEB Deutscher Verlag für Grundstoffindustrie, Leipzig, 1984.
26 P. Bertani, J. Raya and B. Bechinger, *Solid State Nucl. Magn. Reson.*, 2014, **61–62**, 15–18.
27 B. M. Fung, A. K. Khitrin and K. Ermolaev, *J. Magn. Reson.*, 2000, **142**, 97–101.
28 S. Dvinskikh, U. Duerr, K. Yamamoto and A. Ramamoorthy, *J. Am. Chem. Soc.*, 2006, **128**, 6326–6327.
29 S. V. Dvinskikh, U. H. N. Dürr, K. Yamamoto and A. Ramamoorthy, *J. Am. Chem. Soc.*, 2007, **129**, 794–802.
30 S. V. Dvinskikh and I. Furó, *Russ. Chem. Rev.*, 2006, **75**, 497–506.
31 V. I. Chizhik, Y. S. Chernyshev, A. V. Donets, V. V. Frolov, A. V. Komolkin and M. G. Shelyapina, *Magnetic Resonance and Its Applications*, Springer, Heidelberg, 2014.
32 B. M. Fung, in *Encyclopedia of nuclear magnetic resonance*, ed. D. M. Grant and R. K. Harris, Wiley, Chichester, 1996, pp. 2744–2751.
33 M. J. Frisch, G. W. Trucks, H. B. Schlegel, G. E. Scuseria, M. A. Robb, J. R. Cheeseman, G. Scalmani, V. Barone, B. Mennucci, G. A. Petersson, H. Nakatsuji, M. Caricato, X. Li, H. P. Hratchian, A. F. Izmaylov, J. Bloino, G. Zheng, J. L. Sonnenberg, M. Hada, M. Ehara, K. Toyota, R. Fukuda, J. Hasegawa, M. Ishida, T. Nakajima, Y. Honda, O. Kitao, H. Nakai, T. Vreven, J. A. Montgomery, Jr., J. E. Peralta, F. Ogliaro, M. Bearpark, J. J. Heyd, E. Brothers, K. N. Kudin, V. N. Staroverov, T. Keith, R. Kobayashi, J. Normand, K. Raghavachari, A. Rendell, J. C. Burant, S. S. Iyengar, J. Tomasi, M. Cossi, N. Rega, J. M. Millam, M. Klene, J. E. Knox, J. B. Cross, V. Bakken, C. Adamo, J. Jaramillo, R. Gomperts, R. E. Stratmann, O. Yazyev, A. J. Austin, R. Cammi, C. Pomelli, J. W. Ochterski, R. L. Martin, K. Morokuma, V. G. Zakrzewski, G. A. Voth, P. Salvador, J. J. Dannenberg, S. Dapprich, A. D. Daniels, Ö. Farkas, J. B. Foresman, J. V. Ortiz, J. Cioslowski and D. J. Fox, *Gaussian 09, Revision D.01*, Gaussian, Inc., Wallingford CT, 2013.
34 J. W. Emsley, P. Lesot, G. De Luca, A. Lesage, D. Merlet and G. Pileio, *Liq. Cryst.*, 2008, **35**, 443–464.
35 V. S. Neverov, A. V. Komolkin and T. G. Volkova, *Vestn. S.-Peterb. Univ., Ser. 4: Fiz., Khim.*, 2011, **1**, 34–53.
36 T. H. Tong, B. M. Fung and J. P. Bayle, *Liq. Cryst.*, 1997, **22**, 165–169.